

Distributive enzyme binding controlled by local RNA context results in 3' to 5' directional processing of dicistronic tRNA precursors by *Escherichia coli* ribonuclease P

Jing Zhao and Michael E. Harris*

Department of Chemistry, University of Florida, Gainesville, FL 32603, USA

Received August 30, 2018; Revised October 17, 2018; Editorial Decision October 30, 2018; Accepted November 11, 2018

ABSTRACT

RNA processing by ribonucleases and RNA modifying enzymes often involves sequential reactions of the same enzyme on a single precursor transcript. In *Escherichia coli*, processing of polycistronic tRNA precursors involves separation into individual pre-tRNAs by one of several ribonucleases followed by 5' end maturation by ribonuclease P. A notable exception are valine and lysine tRNAs encoded by three polycistronic precursors that follow a recently discovered pathway involving initial 3' to 5' directional processing by RNase P. Here, we show that the dicistronic precursor containing tRNA^{valV} and tRNA^{valW} undergoes accurate and efficient 3' to 5' directional processing by RNase P *in vitro*. Kinetic analyses reveal a distributive mechanism involving dissociation of the enzyme between the two cleavage steps. Directional processing is maintained despite swapping or duplicating the two tRNAs consistent with inhibition of processing by 3' trailer sequences. Structure-function studies identify a stem-loop in 5' leader of tRNA^{valV} that inhibits RNase P cleavage and further enforces directional processing. The results demonstrate that directional processing is an intrinsic property of RNase P and show how RNA sequence and structure context can modulate reaction rates in order to direct precursors along specific pathways.

INTRODUCTION

There are over 80 tRNA genes encoded in the *Escherichia coli* genome. These individual genes are transcribed in the form of 28 monocistronic precursor tRNAs (ptRNAs), 14 polycistronic precursors containing up to seven individual tRNAs, and seven tRNAs are encoded within ribosomal RNA precursors (1) (supplemental data: Table S1, NCBI:

txid511145). The pathways by which these tRNA precursors are processed into mature tRNAs were defined primarily by molecular genetics experiments that characterized the potential intermediates that accumulate in cells depleted of one or more specific tRNA processing enzymes by conditional mutations (2–6). The sequences of these partially processed RNAs supports a general biosynthetic pathway in which processing is initiated by RNase E cleavage within a few nucleotides downstream of each tRNA 3' terminal CCA sequence (4,7). Subsequent endonucleolytic cleavage by the ribonucleoprotein enzyme ribonuclease P (RNase P) is responsible for removal of 5' leader sequence to generate the mature tRNA 5' end (8,9). The process of final 3' terminal maturation as well as *rho* terminator removal is performed by a combination of 3' to 5' exonucleases (6,10,11) (Figure 1A).

In contrast to this canonical pathway for polycistronic tRNA precursor processing, recent molecular genetic studies by Kushner and colleagues demonstrated an alternative processing pathway for three polycistronic precursors that encode the entire complement of valine and lysine tRNAs (valV/valW, valU/valX/valY/lysY and lysT/valT/lysW/valZ/lysY/lysZ/lysQ). This alternative pathway is of particular interest because it involves previously unidentified functions for RNase P which normally acts after separation of individual tRNAs from polycistronic substrates (2) (Figure 1B). Northern blot and primer extension analysis of transcripts that accumulate when RNase P is absent demonstrate that all three polycistronic transcripts undergo initial processing such that separation into individual tRNAs is concomitant with 5' end maturation (2,5). Remarkably, RNase P separates the individual tRNAs by first removing the Rho-independent transcription terminators from the primary valU and lysT transcripts (for clarity the two longest polycistronic substrates are referred to by the tRNA located at their 5' end), and then subsequently catalyzes cleavage proceeding in the 3' to 5' direction generating one pre-tRNA at a time. This unexpected function of RNase P *in vivo* presents several

*To whom correspondence should be addressed. Tel: +1 352 392 0541; Fax: +1 352 392 8758; Email: harris@chem.ufl.edu

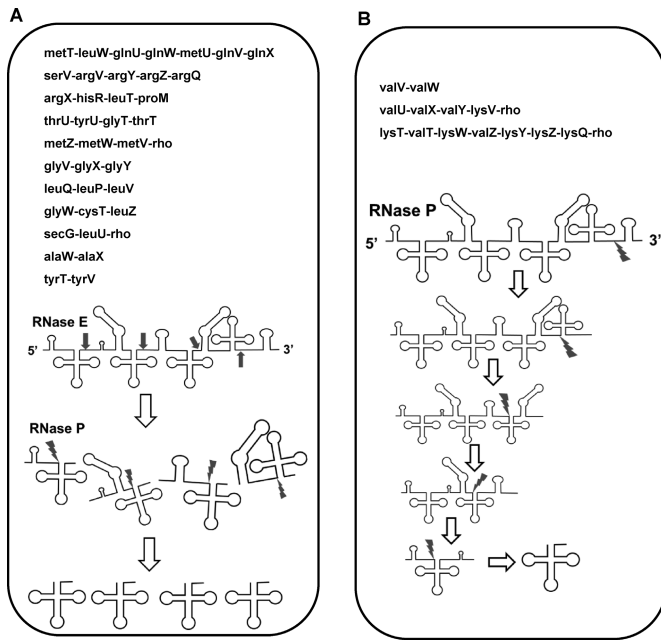


Figure 1. 3' to 5' directional RNase P cleavage is the initial step in processing of three dicistronic tRNA precursors. (A) The eleven polycistronic tRNA precursors are listed that are processed by the major processing pathway in which the initial step is separation into individual monocistronic units by RNase E (indicated by an arrow), 5' end maturation by RNase P (shown as a lightning bolt), and subsequent 3' end trimming (not shown). (B) The three polycistronic tRNA precursors encoding the entire complement of valine and lysine tRNAs undergo initial 3' to 5' directional processing by RNase P, followed by 3' end trimming.

challenges to our current understanding of the substrate specificity of this widespread and essential enzyme. For such a directional processing pathway to occur the rate of processing of the internal RNase P cleavage sites must be suppressed in the primary transcript. These same sites must then become activated for RNase P cleavage subsequent to the processing of the tRNA located immediately downstream. As discussed below, there are several potential mechanisms for such ordered processing, however, the basis for the observed differences in relative rates of phosphodiester bond hydrolysis at different cognate processing sites by RNase P that result in directionality is unknown.

This gap in our knowledge exists despite the fact that the structure of bacterial RNase P and its molecular recognition of several model pre-tRNAs have been well studied (12–14). In most organisms, RNase P occurs as a ribonucleoprotein containing a highly conserved RNA subunit (P RNA) and a single protein or a collection of proteins (13,15). The composition of bacterial RNase P is simplest and is composed of a *ca.* 400 P RNA subunit and a single *ca.* 100 (16) structure that is conserved in all three Kingdoms (17). The folded structure is compact and forms a pocket for contacting the tRNA substrate (16,18–20), which includes an active site that position metal ions for catalysis. P RNA is bound by a single smaller protein subunit of approximately 100 amino acids that contributes to molecular recognition by contacting pre-tRNA 5' leader sequences (21), as well as facilitating P RNA metal ion binding (22,23), and stabilizing structure and conformational changes (24–26). A sub-

set of Eukarya alternatively have one of two classes of protein enzymes as their nuclear or organellar RNase P (13,27). Detailed structure–function studies show that bacterial P RNA recognizes the 11 nucleotide helix formed by the acceptor stem and T-stem and contacts functional groups on the G(1)-C(72) basepair at the tRNA 5' end, the R(73)C(74)C(75) sequence at the 3' end of the tRNA, and N(–1) and N(–2) in the 5' leader sequence. The substrate binding domain of P RNA also contacts 2'-OH groups in the T stem–loop (28,29). The spacing of these contacts in the T stem–loop in relation to the cleavage site results in an overall shape recognition of the substrate (18,30–32). The P protein subunit interactions with the pre-tRNA 5' leader have distinct sequence preferences at positions N(–3) to N(–6), primarily for the nucleobase at N(–4), although this interaction appears to be species-specific (33,34). Despite this detailed understanding of RNase P molecular recognition, none of these features explains the differences processing rate constants at different cognate binding sites that results in 3' to 5' directional processing observed *in vivo* (2,5).

A common feature of RNA processing enzymes including RNase P is the ability to recognize cognate processing sites within different RNA sequence and structure contexts (3,4,11,35–39). There is growing appreciation that the conserved sequences and structures directly contacted by RNA processing enzymes are embedded within a surrounding RNA context that can indirectly influence the relative rates of processing and affinities of RNA binding proteins (40–46). *In vitro* and *in vivo* studies in an increasing number of experimental systems shows that context-dependent effects on RNA recognition can arise due to multiple factors including the presence of competing binding sites (47–52) and the ability to form alternative secondary structures (53–56). Thus, it is important to understand the basis for differences in the relative rates of processing at individual cognate sites in RNA precursors, and how they may contribute to gene expression. With respect to tRNA processing, differences in processing rates can affect steady state tRNA levels in biologically meaningful ways (57–61). The processing of polycistronic RNA precursors by RNase P thus provides a valuable experimental system for investigating molecular recognition of multiple alternative processing sites embedded within a single RNA substrate.

In order to better understand the basis for different rates of processing for different RNase P cleavage sites we investigated the *in vitro* processing of the simplest RNase P-dependent dicistronic precursor substrate (referred to throughout as valVW) which encodes only two substrates, tRNA^{valV} and tRNA^{valW}. The 3' to 5' pattern of processing observed *in vivo* is also observed *in vitro* with synthetic precursor valVW and purified RNase P demonstrating that no additional cellular factors contribute significantly to processing order. Kinetic analyses reveal a distributive mechanism in which directional processing occurs by two independent binding and cleavage steps. Structure–function studies show that inhibition of RNase P cleavage by the presence of long 3' trailer sequences as well as by stable secondary structure in the 5' leader sequence of the upstream tRNA^{valV} are both likely contribute to the observed directional processing mechanism. These data provide insight into a new facets of molecular recognition by an essential tRNA processing

enzyme necessary for understanding its *in vivo* function. Importantly, the data show how processing rates at alternative RNA processing sites may be adjusted by local sequence and structure context.

MATERIALS AND METHODS

Preparation of substrate RNAs and RNase P

The *E. coli* C5 protein was expressed and affinity purified using the NEB IMPACT system as described, previously (62). P RNA and precursor tRNAs were synthesized by *in vitro* transcription from PCR or cloned DNA templates using T7 RNA polymerase, reaction products were purified by denaturing polyacrylamide gel electrophoresis using standard protocols as described (63,64). Pre-tRNA substrates were either 5' end labelled with ^{32}P using γ - ^{32}P -ATP and polynucleotide kinase, or were uniformly labelled during *in vitro* synthesis by including α - ^{32}P -CTP (65) in the reaction followed by gel purification and recovery by ethanol precipitation.

In vitro RNase P processing reactions

Single turnover reactions were performed using a range of enzyme concentrations as described in the text in a reaction buffer containing 50 mM 4-morpholineethanesulfonic acid (MES) pH 6, 100 mM NaCl, 0.005% Triton X-100 and 17.5 mM MgCl_2 . RNase P holoenzyme was assembled in reaction buffer without magnesium by first heat denaturation at 95°C for 3 min followed by incubation at 37°C for 10 min. MgCl_2 was then added to the appropriate concentration and the incubation continued for another 10 min. A 1.5X equivalent concentration of C5 protein relative to the P RNA concentration was added to form the RNase P holoenzyme. Substrate solutions were prepared separately using ^{32}P -labeled pre-tRNA by the same protocol. Equal volumes (*ca.* 40 μl) of RNase P holoenzyme and ptRNA substrate were mixed to begin the reaction. The final concentrations of RNase P were 10 nM–1 μM and ptRNA substrate concentration < 1 nM. Aliquots (~5 μl) were taken during the time courses and quenched with equal volume of formamide loading dye containing 100 mM EDTA. Substrate and products were separated by electrophoresis on 15% denaturing polyacrylamide gels and each band was quantified by phosphorimager. The resulting data were used to calculate conversion of substrate to product which was plotted versus time and fit to the appropriate rate equations described, below.

Analysis of reaction kinetics

The decrease in substrate concentration for both monocistronic and dicistronic substrates followed simple pseudo first order kinetics and rate constants were determined by fitting the decrease in substrate concentration to Equation (1).

$$F(\text{fraction reaction}) = 1 - Ae^{-kt} \quad (1)$$

where F is the fraction of total substrate remaining ($F = [S]/([P]+[S])$) at each time point. The term A is the amplitude of the reaction and k is observed rate constant and t is



Scheme 1. Consecutive first order reaction.

time. Rate constants were obtained from at least three independent repeats with error bars shown in the figures representing one standard deviation.

In order to quantify the observed rate constants for cleavage of the native dicistronic valVW substrate that contains two cleavage sites, the reaction was fit to a mechanism involving two sequential first order reactions (66), as illustrated in Scheme 1.

In Scheme 1, the species **a**, **b** and **c** are identified in Figure 3 and correspond to the 5' end labeled valVW substrate, the 5' valW cleavage product, and the 5' leader of valV, respectively. The data for the decrease in 5' end labeled valVW substrate (**a**) was fit to a single exponential function (Equation 1) to determine the observed rate constant for processing at the valW site (k_1). To independently determine k_1 and confirm its magnitude the data for the accumulation and decay of the intermediate species **b** was fit to Equation (2).

$$F(b) = \frac{k_1}{(k_2 - k_1) * (e^{-k_1 t} - e^{-k_2 t})} \quad (2)$$

In this equation, $F(b)$ is fraction of the total substrate in the intermediate **b** form ($F(b) = \mathbf{b}/(\mathbf{a} + \mathbf{b} + \mathbf{c})$) and k_1 and k_2 are defined in Scheme 1. The magnitude of k_1 was determined in two ways. First, by fitting the depletion of substrate (**a**) to Equation (1) and by using Equation (2) and fitting the signal obtained from quantifying the intermediate product **b**. The magnitudes of k_1 obtained from these two analyses was typically within 20%. Similarly the magnitude of k_1 was determined by fitting the intensity of the signal for intermediate **b** to Equation (2) as well as by fitting the accumulation of product **c** to Equation (3).

$$F(c) = 1 - \frac{k_2 * e^{-k_1 t} - k_1 * e^{-k_2 t}}{k_2 - k_1} \quad (3)$$

In this equation $F(c)$ is fraction of the total substrate in the product **c** form ($F(c) = \mathbf{c}/(\mathbf{a} + \mathbf{b} + \mathbf{c})$) and k_1 and k_2 are defined in Scheme 1. For evaluation of k_2 using this method the magnitude of k_1 was fixed to the value obtained from fitting the data from the same reaction to Equations (1) and (2).

In-line probing

In-line probing assays were used to assess the formation of native secondary structure for the valVW dicistronic substrate and synthetic substrates with swapped or duplicated tRNAs (67). Briefly, 5' ^{32}P -labeled substrate RNAs synthesized using the protocol described, above, was incubated in in-line reaction buffer [50 mM Tris-HCl, pH 8.3, 20 mM MgCl_2 and 100 mM KCl] at room temperature (20°C) for 40 h, 3 μl of reaction was loaded in both 8% and 12% denaturing gel running at 40 W for 3.5–4 h, gels were dried and exposure to phosphorimager plates. RNase T1 reaction was incubated in sodium citrate buffer [0.025 M sodium citrate,

pH 5.0 at 23°C] for 5 min, 3 μ l of reaction was loaded as a marker to allow the nucleotide position corresponding to gel individual bands to be identified. Alkaline digestion reaction was incubated in Na₂CO₃ buffer [0.05 M Na₂CO₃, pH 9.0 at 23°C and 1 mM EDTA] at 90°C for 5 min. 3 μ l of the alkaline hydrolysis reaction was loaded on the gel to serve as a marker.

Pulse-chase analysis of reaction processivity

For the pulse-chase experiments shown in Figure 6 an isotope dilution approach was used in which the reaction was initiated with a low concentration of labeled substrate and then a high concentration of unlabeled substrate was added at an intermediate time during the reaction (68). The kinetics before and after the non-radiolabeled substrate chase were compared to determine the degree to which the enzyme dissociates between processing events on the same substrate. An individual single turnover reaction condition containing 30 nM RNase P and *ca.* 1 nM valVW dicistronic precursor substrate was set up as described, above. After mixing enzyme and substrate the reaction was allowed to proceed and then divided into two parallel reactions when \sim 30% of the initial substrate was consumed. For one of the parallel reactions, the reaction was continued as usual and 5 μ l aliquots were taken at each time point. For the second reaction, 1 μ l of a high concentration of RNA competitor (the native dicistronic valVW substrate) to a concentration of 60 μ M was added to quench the reaction. The products of both reactions were resolved on 15% denaturing polyacrylamide gels.

RESULTS

Evidence for 3' to 5' ordered processing of dicistronic ptRNA_{valV} by RNase P *in vitro*

The valVW substrate provides a simple model system to determine the basic mechanistic features that underlie directional processing. This dicistronic precursor is relatively small (178 nucleotides) and contains two valine tRNAs (tRNA^{valV} and tRNA^{valW}) substrates from isotype 1 that differ only by a few nucleotide positions in the acceptor stem as shown in Figure 2A. There are four nucleotides in the intergenic region between the two tRNAs that lacks a classic A/U rich RNase E cleavage site. The tRNA^{valV} at the 5' end has a 20 nucleotide long leader sequence. Inspection of the tRNA^{valV} 5' leader sequence shows that it most likely forms a stable 6 pair nucleotide stem with a 5-nucleotide loop located two nucleotides away from RNase P cleavage site. Recent comprehensive analysis of the sequence specificity of C5 protein shows that RNA structure as well as sequence preferences in the 5' leader affects the k_{cat}/K_m for RNase P cleavage(34). RNase P recognizes the folded structure of tRNA, and given the highly self-complementary sequence of the dicistronic valVW folding into alternative conformations could affect the reaction kinetics observed *in vitro*. Therefore, it is critical to first test for formation of the predicted 5' stem loop and establish the predominant folded conformation of the *in vitro* transcribed dicistronic valVW substrate.

In-line probing involves analysis of the pattern of spontaneous cleavage of the phosphodiester backbone of 5' end labeled RNA in which enhanced reactivity reflects backbone structure with correct geometry for in-line attack (67). Figure 2 shows that the valVW substrate produces an in-line probing pattern that is consistent with the predicted secondary structure. Cleavage at tRNA loops and junction regions are clearly observed (Figure 2A) which precisely corresponds to loops and bulges in the precursor (Figure 2B and C). Predicted stems appear to be well formed and protected from in-line attack. G39 in the D-loop is clearly protected from in-line attack, consistent with long-range tertiary base-pairing with C77 in the T-loop. Although it is difficult to map the 10–15 nucleotides near the extreme 3' end of tRNA^{valW} (lower-case in Figure 2), the data clearly shows that the acceptor stem and D-stem of tRNA^{valW} are correctly formed.

Analysis of the processing kinetics of the valVW dicistronic substrate was performed under single turnover reaction conditions as described in Materials and Methods. These conditions are chosen to simplify the interpretation of the kinetics of the formation and decay of intermediates, and to allow the reaction rate constants to be quantified without complication due to product inhibition. For an optimal ptRNA^{met} substrate the rate constant for substrate dissociation is slow and the observed state constant at saturating enzyme concentrations reflects substrate association (69). However, this mechanism may not hold for substrates like valVW with more complex structures and potential inhibitory secondary structure. Figure 3 shows the products formed by *in vitro* processing of 1 nM 5' ³²P-labeled dicistronic valVW substrate by 30 nM RNase P. Since the radiolabel is uniquely located on the RNA 5' end only the original substrate (species **a** in Figure 3), and reaction intermediates and products that retain the original substrate 5' phosphate can be detected. The apparent kinetics of formation of reaction products visualized by phosphorimager analysis appears to reproduce the 3' to 5' directional processing of valVW observed *in vivo* (Figure 3A and B). The intermediate **b** contains the original 5' end ³²P label and it is formed at early time points. The mobility of this product is consistent with cleavage in the intergenic region at the correct valW processing site. Intermediate **b** disappeared with similar apparent kinetics as the accumulation of product **c** that has mobility in the gel consistent with correct cleavage at the 5' tRNA^{valV} processing site. These results are consistent with a simple sequential mechanism (Scheme 1) in which the substrate **a** is converted to intermediate **b** that is processed to yield 5' product **c**.

A sequential mechanism is further supported by fitting the data to Equations (1)–(3) derived for Scheme 1 (66) and quantification of the observed rate constants k_1 and k_2 . As described in Materials and Methods the magnitude of k_1 obtained by fitting the decrease in substrate **a** is consistent with the kinetics of intermediate **b** formation and the lag in formation of product **c**. Similarly, the magnitude of k_2 that is obtained by fitting the kinetics of the decay of intermediate **b** is consistent with the formation of product **c**. In sum, the fitting results show that valVW is processed by RNase P by initial fast cleavage at the 3' most valV tRNA site ($k_{obs}(valV)$: 0.013 ± 0.002 s⁻¹) followed by processing

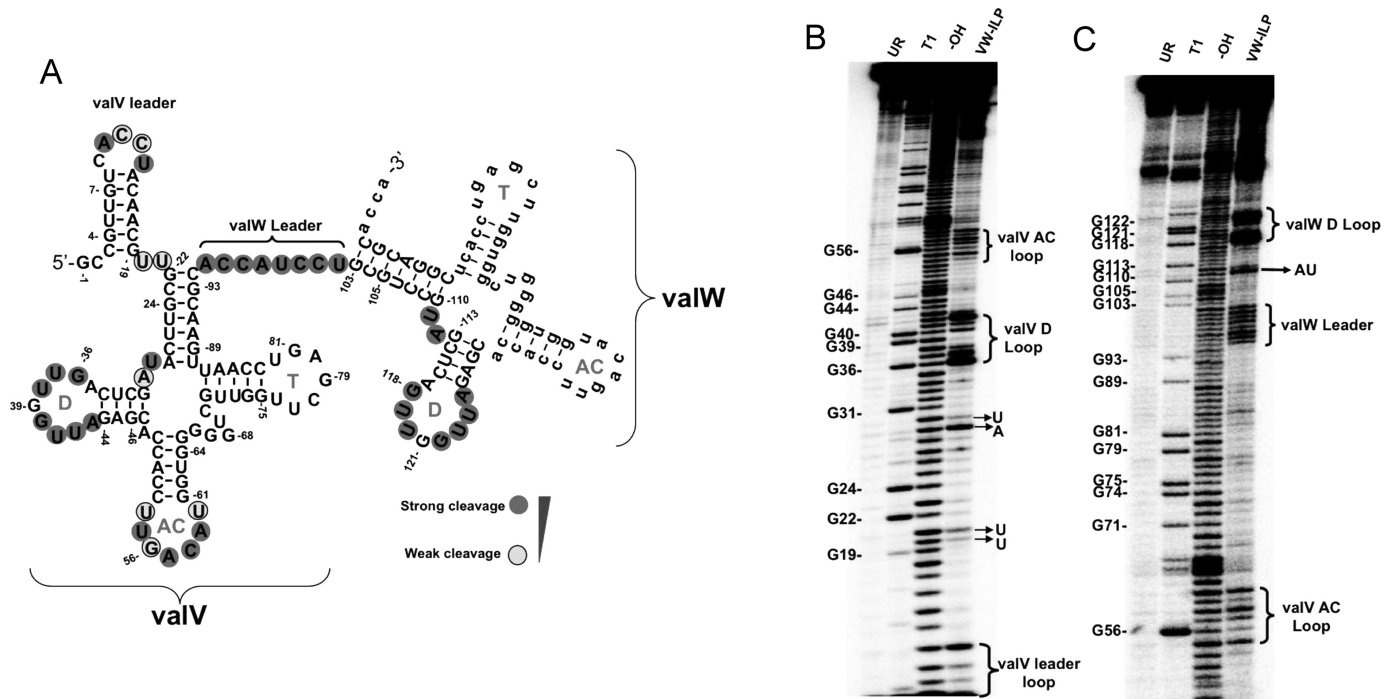


Figure 2. In-line structure probing of 5' ^{32}P end-labeled dicistronic valVW precursor RNA corresponds to predicted secondary structure. (A) Predicted secondary structures of the valVW substrate. Levels of spontaneous RNA cleavage at backbone are circled and shaded according to the intensity of the cleavage product. Analysis of valVW cleavage products on 12% (B) and 8% (C) polyacrylamide gels. Lanes are marked as follows. UR: unreacted RNA; T1: partial RNase T1 digestion; OH: partial alkaline hydrolysis; VW-ILP: refolded ptRNAs^{val} VW subjected to in-line probing condition (50 mM Tris-HCl (pH 8.3 at 20°C), 20 mM MgCl₂, and 100 mM KCl) incubated in 21°C for 40 h. Bands corresponding to sites of T1 digestion are numbered as indicated in panel A.

at the 5' most valW tRNA site with an equivalent apparent rate constant ($k_{\text{obs}}(\text{valW}): 0.029 \pm 0.002 \text{ s}^{-1}$).

To characterize the entire complement of reaction intermediates and products we repeated the kinetic experiments using an RNA substrate population synthesized *in vitro* using [α - ^{32}P] CTP so that the resultant RNAs are uniformly labelled (Figure 3C). The full length valVW (a) was again processed to generate intermediate b that retains the 5' end as well as 3' products c2 and c3 that form with similar apparent kinetics (also see scheme in panel D). The c2 and c3 products are *ca.* 77 nucleotides in length consistent with the mature tRNA^{valW}. Based on 5' end mapping results (see below) the different products are due to 3' end heterogeneity generated during *in vitro* transcription by T7 RNA polymerase (70,71). The intermediate b decreases as expected at later time points and is further cleaved to generate product c1, which is *ca.* 81 nucleotides in length and represents the mature tRNA^{valV} with the additional UCCU intergenic sequence at the 3' end (scheme in panel D, bottom line). The corresponding 5' leader fragment generated by the second cleavage reaction migrates lower in the gel and is not shown on in the figure. A very minor high molecular weight product is also observed that is consistent with a minor (<1%) amount of initial cleavage at the 5' tRNA^{valV} site. Therefore, the data from uniformly labelled RNA verifies the identity of predicted cleavage products from dicistronic valVW processing by RNase P and is fully consistent with a 3' to 5' directional processing mechanism.

Next, we confirmed the site-specificity of RNase P processing at both cleavage sites in valVW. As shown in Figure 4, five time points collected during the reaction were loaded next to RNase T1 cleavage standards that map G residues, and an alkaline hydrolysis digestion ladder. The nucleotides around each cleavage site are mapped as marked on the secondary structure of valVW (Figure 2A) and marked next to gel in Figure 4. The cleavage events resulting in the major products (Figure 3A, products b and c) were verified as resulting from correct processing by RNase P at the authentic 5' ends of tRNA^{valW} and tRNA^{valV} tRNA, respectively.

Kinetic evidence for a distributive processing mechanism

The directional processing pathway observed for valVW may occur due to several potential mechanisms. In a simple distributive mechanism binding occurs independently to the two sites, and the presence of additional 3' sequences or some other feature is inhibitory, thereby blocking cleavage at the tRNA^{valV} site until cleavage at the downstream tRNA^{valW} site has occurred. A second model that is consistent directional processing is a processive mechanism in which RNase P binds initially at the 3' end and scans the substrate in a 3' to 5' manner without dissociation to identify potential cleavage sites. (Supplementary Figure S1, see Supplementary Information 'Simulation of processive and distributive mechanisms for *E. coli* RNase P Processing of precursor valVW')

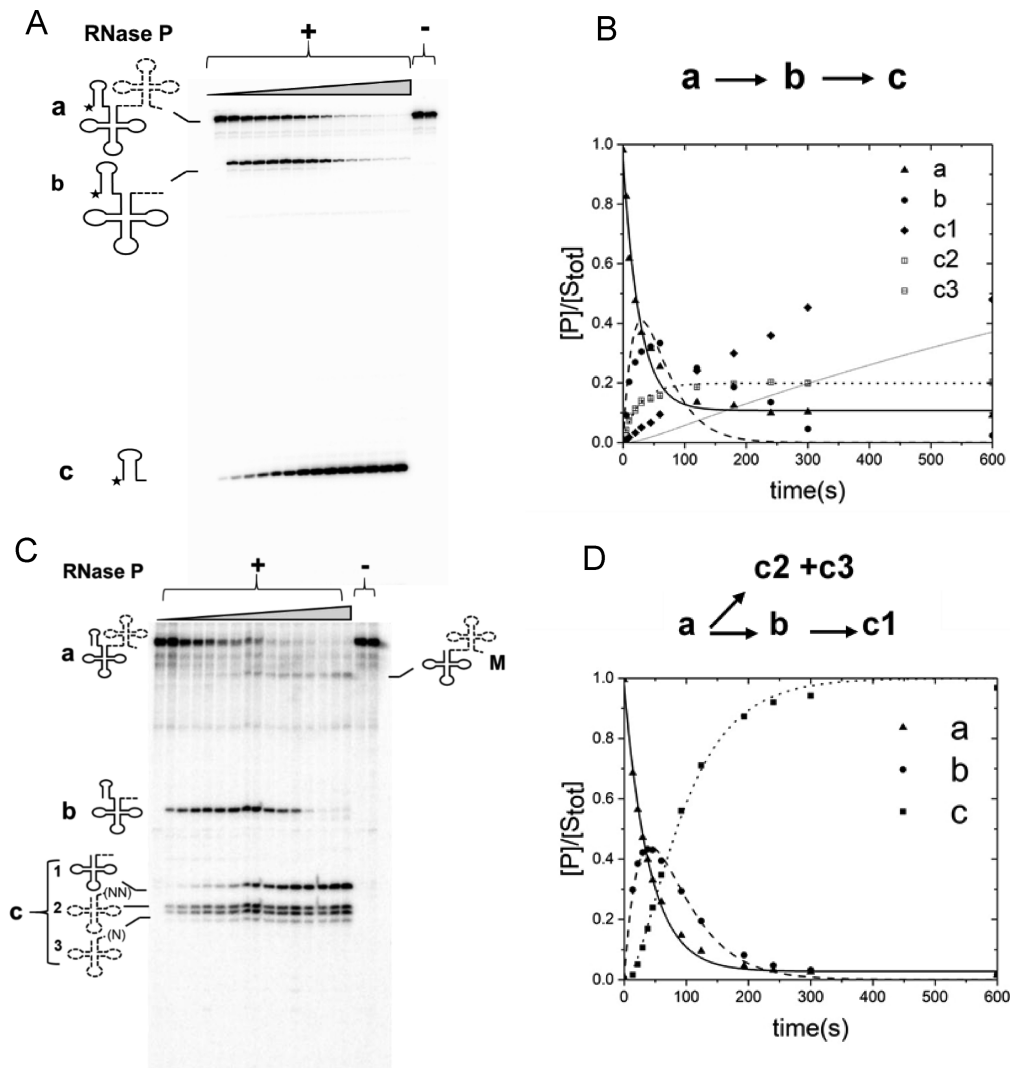


Figure 3. *In vitro* processing of of 5' ^{32}P end-labeled (A) and uniformly labeled with α - ^{32}P -CTP (C). Reactions either containing or lacking RNase P are marked by plus (+) or minus (-) symbol, respectively. Structures of the substrate and predicted structures of products are shown next to each band based on gel mobility. The tRNA^{valV} is shown as a black line and the tRNA^{valW} is shown as a dashed line. Total incubation time for substrate is shown as an oblique triangle (30 minutes). (B). Fitting of the change in fraction of the substrate **a**, intermediate **b**, and product **c** to equations for two sequential first order reactions. As described in Materials and Methods, the data for **a** are fit to equation 1 is shown as a dashed line, the data for **b** and **c** are fit to Equations (2) and (3), respectively.

Simple processive (Scheme 1, processive) and distributive models (Scheme 2, non-processive) for valVW directional processing by RNase P are illustrated in Figure 5A. In the processive mechanism RNase P (E) binds the valVW substrate (S) at the downstream tRNA^{valW} cleavage site with equilibrium constant K_A and cleavage occurs at k_1 . Processing at the tRNA^{valV} site occurs subsequently with rate constant k_2 without dissociation and equilibration of RNase P with the free enzyme population. In the distributive mechanism, binding occurs to the tRNA^{valW} cleavage site as in the processive mechanism, however, for processing at the tRNA^{valV} site enzyme dissociation, and rebinding with equilibrium constant K_B occurs followed by processing with rate constant k_2 . Importantly, the products predicted for initial cleavage at the tRNA^{valV} site are not observed. Thus, the relative second order rate constant for cleavage at this site must be significantly slower (>10-fold) in the

valVW substrate compared to the rate of cleavage at the tRNA^{valW} site. An important distinction between the two mechanisms is clearly the presence of an independent binding step in the distributive mechanism. Thus, it follows that a fundamental difference in the observed reaction kinetics will be the enzyme concentration dependence of the observed rate constant for the second cleavage step. Accordingly, we performed a series of reactions with a range of enzyme concentrations (10–600 nM) and quantified the observed rate constants for processing at the tRNA^{valV} (k_1) and tRNA^{valW} (k_2) sites. A plot of the observed k_1 and k_2 versus RNase P concentration is shown in Figure 5B shows that cleavage at both sites are concentration dependent and show saturation behavior at enzyme concentrations greater than 60 nM and an apparent equilibrium constant K_{obs} of ca. 10 nM.

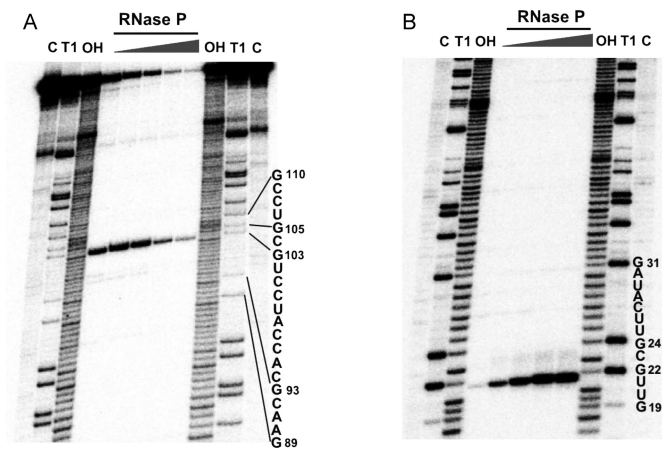


Figure 4. Site specificity of RNase P processing of the dicistronic valVW precursor *in vitro*. Phosphorimager analysis of cleavage products resolved on 8% (A) and 12% gel (B) polyacrylamide gels with 5' ³²P end-labeled valVW RNA. The lanes are marked as follows. (C) Control reaction with no enzyme, OH: alkaline hydrolysis of dicistronic valVW, T1: RNase T1 ladder. The positions of the guanosines and surrounding sequence are indicated next to the gel.

A second consequence of the difference in the processive *versus* distributive mechanisms is the level of accumulation of intermediate product **b**, which results from initial cleavage at the downstream tRNA^{valW} cleavage site. In the processive mechanism **b** accumulates to a lesser degree at low enzyme concentrations compared to saturating enzyme concentration due to the change in relative magnitudes of the rate constants for the first and second cleavage steps. In contrast, **b** accumulates to the same extent since the rate constants for both steps increase with increasing enzyme concentration, but their relative magnitudes will remain the same. To illustrate this principle kinetic simulations of the processive and non-processive mechanisms were performed using the estimates of rate and equilibrium constants observed for the native substrate as described in Supplementary Information. As shown in Figure 5C for the *in vitro* processing of valVW the intermediate **b** accumulates to approximately the same extent at both limiting and saturating enzyme concentration. This result, together with the dependence of k_1 and k_2 on enzyme concentration are clearly most consistent with the non-processive mechanism involving independent binding and cleavage at both sites.

Next, we tested whether RNase P equilibrates with the free enzyme population between processing at the tRNA^{valW} and tRNA^{valV} sites as predicted by the distributive mechanism using an 'isotope trapping' experiment (68). The RNase P-valVW complex was formed by mixing limiting substrate (1–2 nM) with a saturating concentration of enzyme (60 nM). At an intermediate time, an excess of non-radiolabeled valVW substrate was added. If RNase P does not dissociate between cleavage steps then there will be no corresponding effect on reaction kinetics in the presence or absence of the non-radiolabeled valVW 'chase'. Alternatively, if RNase P dissociates from the substrate after the first cleavage step, then the addition of non-radiolabeled substrate will slow the conversion of intermediate **b** to product **c**. As shown in Figure 6, the presence of competitor

valVW substrate alters the reaction kinetics and dramatically slows the second cleavage step, which further demonstrates a dissociative mechanism. In sum, the concentration dependence of the observed rate constants for processing at the tRNA^{valV} and tRNA^{valW} sites, the enzyme concentration dependence of intermediate **b** accumulation, as well as the response to the presence of excess substrate in pulse-chase experiments demonstrate a distributive mechanism.

Kinetics of RNase P processing of swapped and duplicated tRNA are consistent with inhibition by 3' trailer sequences

In order for directional processing to occur by a distributive reaction scheme, the rate of cleavage at the upstream tRNA^{valV} site must be suppressed in the dicistronic valVW substrate. A simple mechanism for the observed directional processing is inhibition of cleavage at the upstream tRNA^{valV} site by the presence of a specific sequence or structure in tRNA^{valW} as part of the 3' trailer sequence. To test this prediction, we generated three novel dicistronic ptRNAs constructs in which the order of the tRNAs and associated 5' leaders are swapped (valVW) or in which they are duplicated (valVV and valWW). Single turnover reactions were performed and the observed cleavage sites were mapped for each substrate. The kinetics of dicistronic valVW, valVV and valWW processing by the RNase P holoenzyme were quantitatively analysed and compared with genomic encoded dicistronic ptRNA^{val} VW.

Dicistronic ptRNA^{val} VW in which the order of tRNAs are swapped (Figure 7A) shows comparable kinetics with a pattern of intermediates and products that are similar compared to the native dicistronic ptRNA^{val} VW substrate (Figure 3A). Intermediate **b** is the only species that appears in the gel at very early time points and it decays at later time points with concomitant formation of product **c**. These data indicate RNase P processing at the 3' end valV cleavage site first followed by cleavage at the upstream valW site. The two cleavage sites were verified as occurring at the correct tRNA 5' end by T1 mapping (see Supplementary Information, Figure S2). The pattern of products and reaction kinetics are clearly consistent with directional processing in which the 3' most processing site on both dicistronic ptRNA^{val} VW and WV substrates is cleaved first in a manner that is independent of the tRNA identity or the associated 5' leader sequences. Fitting the data for the swapped valVW substrate to equations for a sequential first order mechanism shows that this general mechanism is followed (Figure 7A).

The reaction products and kinetics were similarly analysed for the dicistronic valVV and valWW substrates in which the individual ptRNA valV and valW with their associated 5' leader sequences are duplicated. For the valVV substrate, approximately 90% of precursor is reacted. However, products **b** and **c** accumulated at the same time and with similar kinetics since both of them fit to a single exponential curve (Figure 7B). The size of both product **b** and **c** are consistent with cleavage at the correct site for the 3' and 5' end substrate respectively (Supplementary Figure S3). The observation that both species **b** and **c** accumulated with similar rate constants is inconsistent with the 3' to 5' directional processing. Rather, the valVV substrate appears to be processed at both sites randomly with similar rate con-

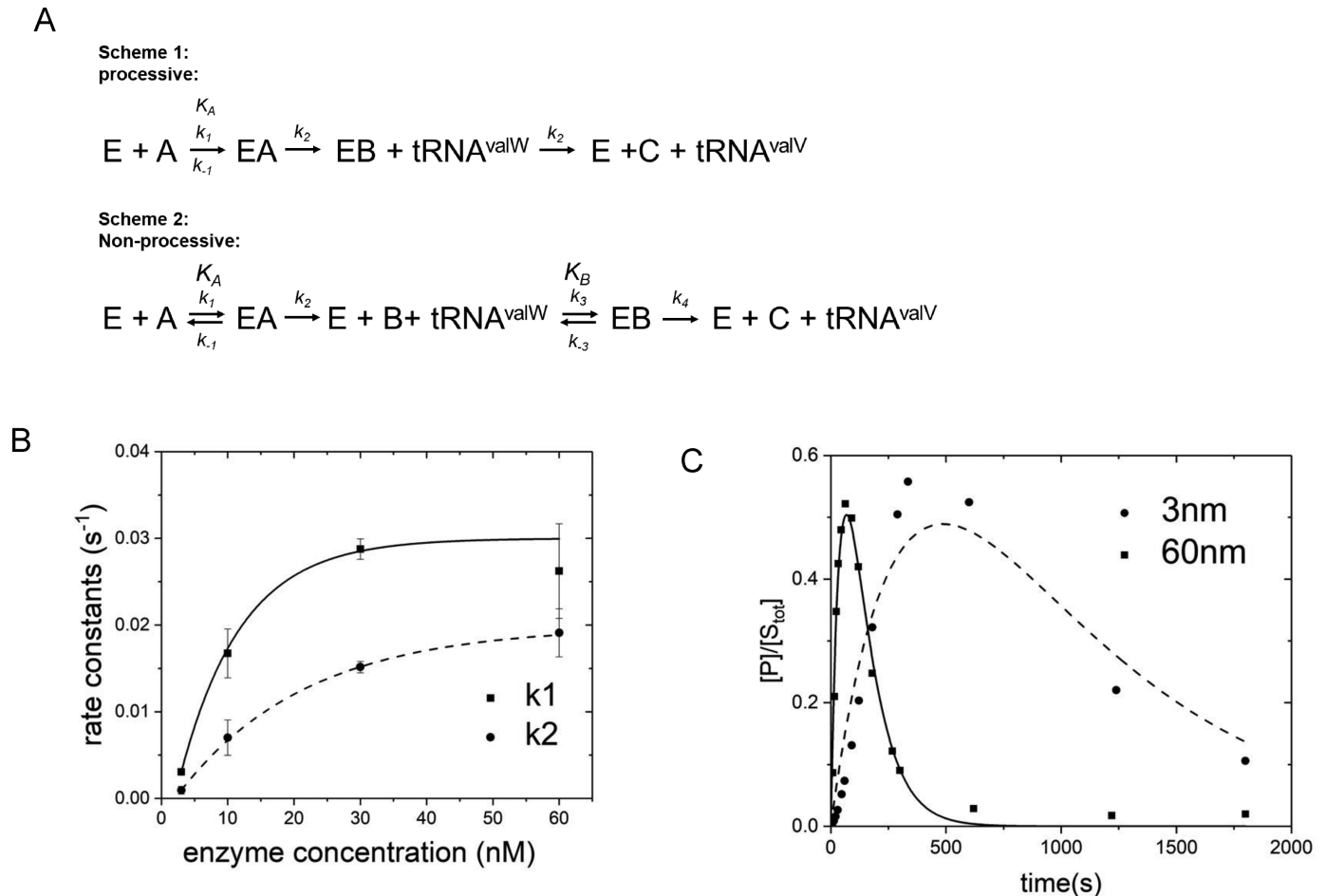


Figure 5. Dependence of the observed rate constants and accumulation of reaction intermediate as a function of enzyme concentration. (A) Two possible mechanisms for RNase P processing of dicistronic ptRNA^{val} VW. In the first model the processing of the two sites is processive (Scheme 1, processive) without dissociation of the enzyme between the two cleavage events, and the second is a distributive model (Scheme 2, non-processive) in which processing at the two sites occurs independently. (B) Dependence of k_1 and k_2 for 3' to 5' directional processing of valVW on RNase P concentration under single turnover reaction conditions (Materials and Methods). (C) Comparison of the accumulation intermediate **b** in reactions containing high (60 nM) and low (3 nM) enzyme concentration showing accumulation to the same extent independent of enzyme concentration.

stants. Importantly, the species **b** resulting from cleavage at 3'-proximal cleavage site remains stable and does not undergo further processing to form product **c**. These data reveal two important insights. First, the presence additional 3' trailer sequences is not uniformly an inhibitor of RNase P processing, since rapid processing at the upstream cleavage can occur in the presence of a 3' trailer sequence containing a tRNA. Second, lack of subsequent cleavage of the product **b** suggests that upstream processing site is likely to be inhibited by misfolding. The products observed and the kinetics of their accumulation show that the valVV substrate appears to be processed by RNase P at both sites in a mutually exclusive manner and not from the 3' to 5' direction.

The reaction of 5' ³²P end-labelled valWW substrate yields only the single, small product **c** representing the 5' leader resulting from cleavage at the upstream tRNA^{valW}. However, over 60% of the initial substrate remained unreacted even at long incubation times (Figure 7C). This result indicates that a large fraction of the valWW RNA folds into a conformation that is not recognized as a substrate by RNase P. The remaining fraction of the valWW

substrate population is reactive and undergoes faster cleavage at the RNase P processing site located near the 5' end rather than the 3' end. Again, this result demonstrates that the presence of 3' trailer sequences is not uniformly inhibitory, and together with the results described above for the valVV substrate, suggests that duplicated tRNA substrates are prone to misfolding resulting in multiple RNA conformations with different reactivities.

Thus, the kinetics results suggested that the dicistronic ptRNA^{val} VV and WW form mis-folded RNA conformations. Therefore, we subjected each dicistronic ptRNAs (valWV, valVV and valWW) to in-line probing to test the extent to which they fold *in vitro* as expected. Indeed, as shown in Figure 8 the in-line probing pattern of valWV is not entirely consistent with the predicted secondary structure. Specifically, there are deviations from the predicted structure in the stem loop between the two tRNAs that forms the leader structure of the 3' tRNA^{valV} cleavage site. With respect to the 5' tRNA^{valW} the pattern of in-line cleavage products is as expected based on the secondary structure: the D-loop, helix junctions, anticodon, T-loop show

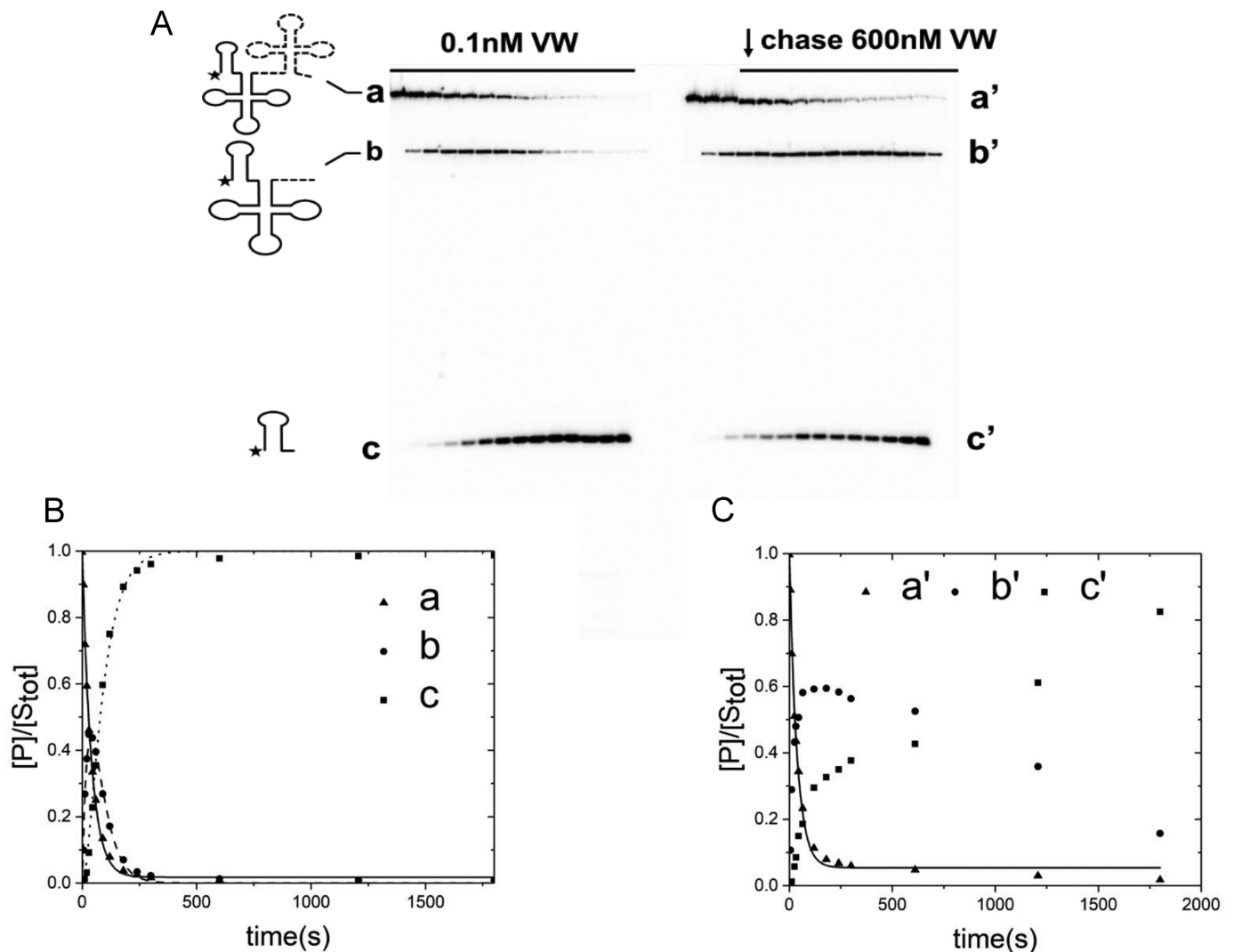


Figure 6. Determination of the reversibility of binding at the 5' tRNA valV processing site. (A) Time courses of processing of 5' ^{32}P -labeled dicistronic valVW precursor by RNase P under single turnover conditions without (left) or with (right) addition of excess unlabeled valVW substrate after $\sim 30\%$ of radiolabeled substrate had been cleaved at the 3'-proximal site. (B and C) The kinetics of substrate a, intermediate b and 5' leader fragment c are fit to equations for two sequential first order reactions for both data sets to illustrate the change in reaction kinetics post-chase.

cleavage and predicted stems are protected (Figure 8A and B). However, pronounced cleavage is observed in the predicted intergenic stem loop in the leader structure of the 3' tRNA^{valV}. The in-line cleavage observed in the predicted intergenic stem loop suggests local mis-folding, or heterogeneity in the pairing pattern within this stem. The acceptor stem of tRNA^{valV}, and the intergenic stem are both GC rich and multiple alternative pairings are possible in the intergenic region. These results can be compared with the kinetic data obtained using dicistronic valVW in which accurate and efficient 3' to 5' directional processing is nonetheless observed. Although the intergenic region between the two substrates appears to be mis-folded, or to assume a population of structures, they are compatible with fast cleavage by RNase P. Independent of structure in the intergenic region in between, the RNase P enzyme still processes the dicistronic valVW RNA in a 3' to 5' directional manner like the native valVW substrate.

The in-line probing pattern of the duplicated valVW substrate is consistent with predicted secondary structures of the encoded tRNAs (Figure 8C and D). Cleavage at the 5' leader loop (only a part of the loop shown in the gel) and at the adjacent sequences 'UU' from G19–G22 confirmed the formation of the stem loop in the 5' leader of the upstream tRNA^{valV}. The single strand leader sequence of 3' end valV 'CCAC' and U117–U118 shows strong spontaneous cleavage as well as the 3' leader loop from C106–U110. No cleavage in the gel from region C100 to G116 is observed. Together, these confirmed the formation of the stem loop in the 3' leader structure of the downstream tRNA. Cleavage at positions U29–A30, A35–A43, U54–U60, G66–C70, U126–A127, A132–A140, these regions correspond to single strand nucleotides or bulges. Taken these together, dicistronic valVW folds correctly in general as predicted.

The in-line probing pattern of valVW, however, suggests that duplication of two identical tRNAs within one di-

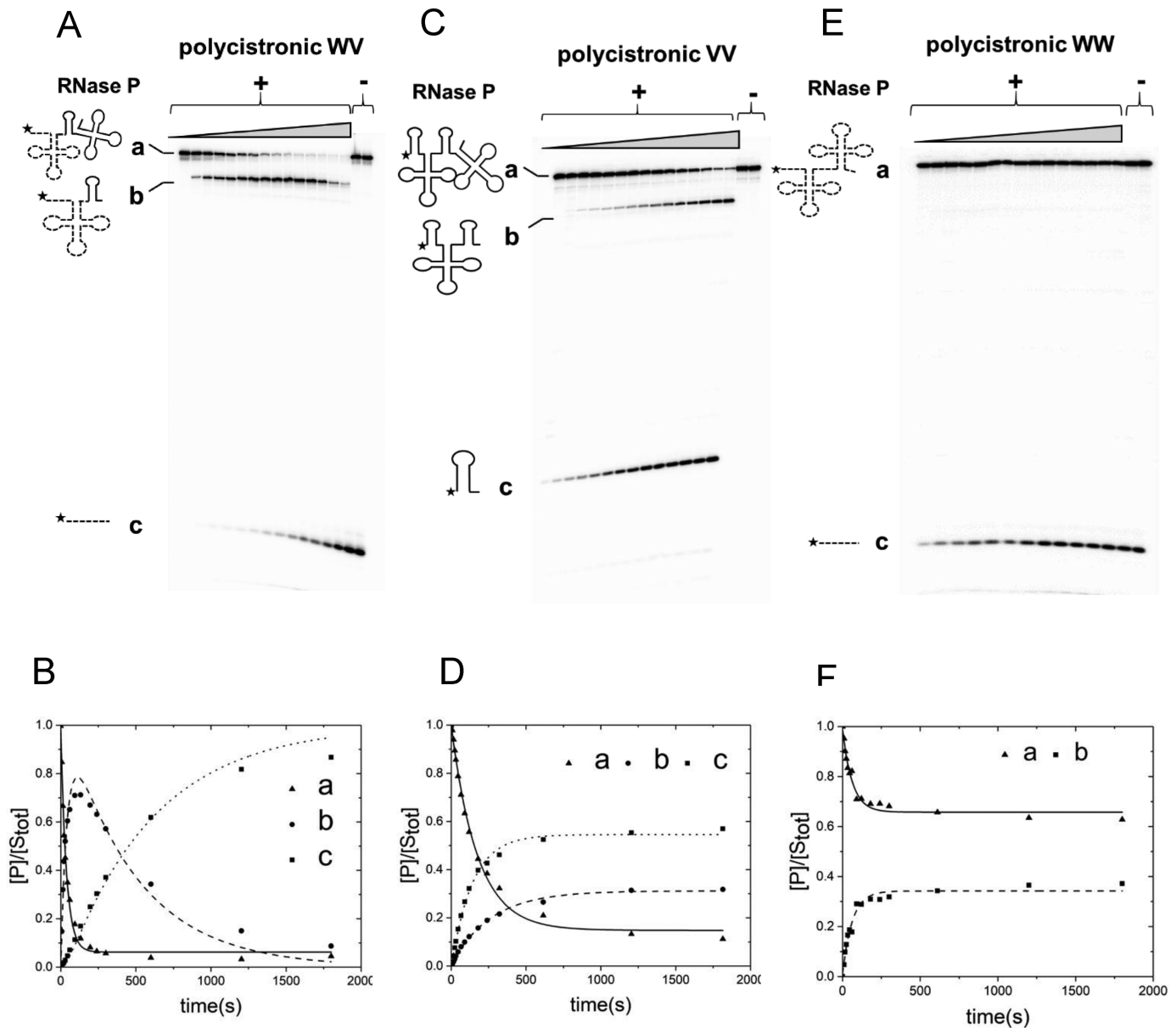


Figure 7. Kinetics analysis RNase P processing of 5' 32 P-labeled dicistronic valWW (A and B), valVV (C and D) and valWV (E and F) substrate RNAs. Single turnover reactions were performed as described for the native valVV substrate. The position of cleavage resulting from processing at the correct sites is supported by T1 mapping (see Supplementary Figures S3–S5). The structure of substrates and products are shown next to each band. The tRNA^{valV} is shown as a black line and the pRNA^{valV} is shown as a dashed line. Incubation time for each substrate is shown as an oblique triangle (30 min). Panels B, D and F show quantitative analysis by fitting the data for each reaction to equations for sequential first order reactions as described in Material and Methods.

cistronic transcript can result in significant mis-folding. As shown in Figure 8, the 5' end tRNA^{valW} appears to fold correctly. Cleavage are only observed in U16–A17, D loop and AC loop. The T loop of 5' end valW, however, is well protected in the structure. We also observe limited T1 digestion at positions G76–G96 suggesting formation of highly stable secondary structure corresponding to the two identical acceptor stems. We hypothesize that the acceptor stems of the two tRNA^{valW} sequences may undergo alternative folding in which the 5' end tRNA^{valW} acceptor stem base pairs with the complementary 3' end of the second downstream tRNA^{valW} acceptor. This possible folding pattern is consis-

tence the formation of a single product with an accurate RNase P cleavage at the 5' end tRNA^{valW} site (Supplementary Figure S4).

A stable stem loop in the tRNA^{valW} 5' leader inhibits RNase P cleavage and further enforces directional processing

To better understand the origin of the large differences in rate constants for processing at the valV and valW cleavage sites in different dicistronic contexts, we measured the reaction kinetics of monocistronic tRNA^{valV} and tRNA^{valW} pre-

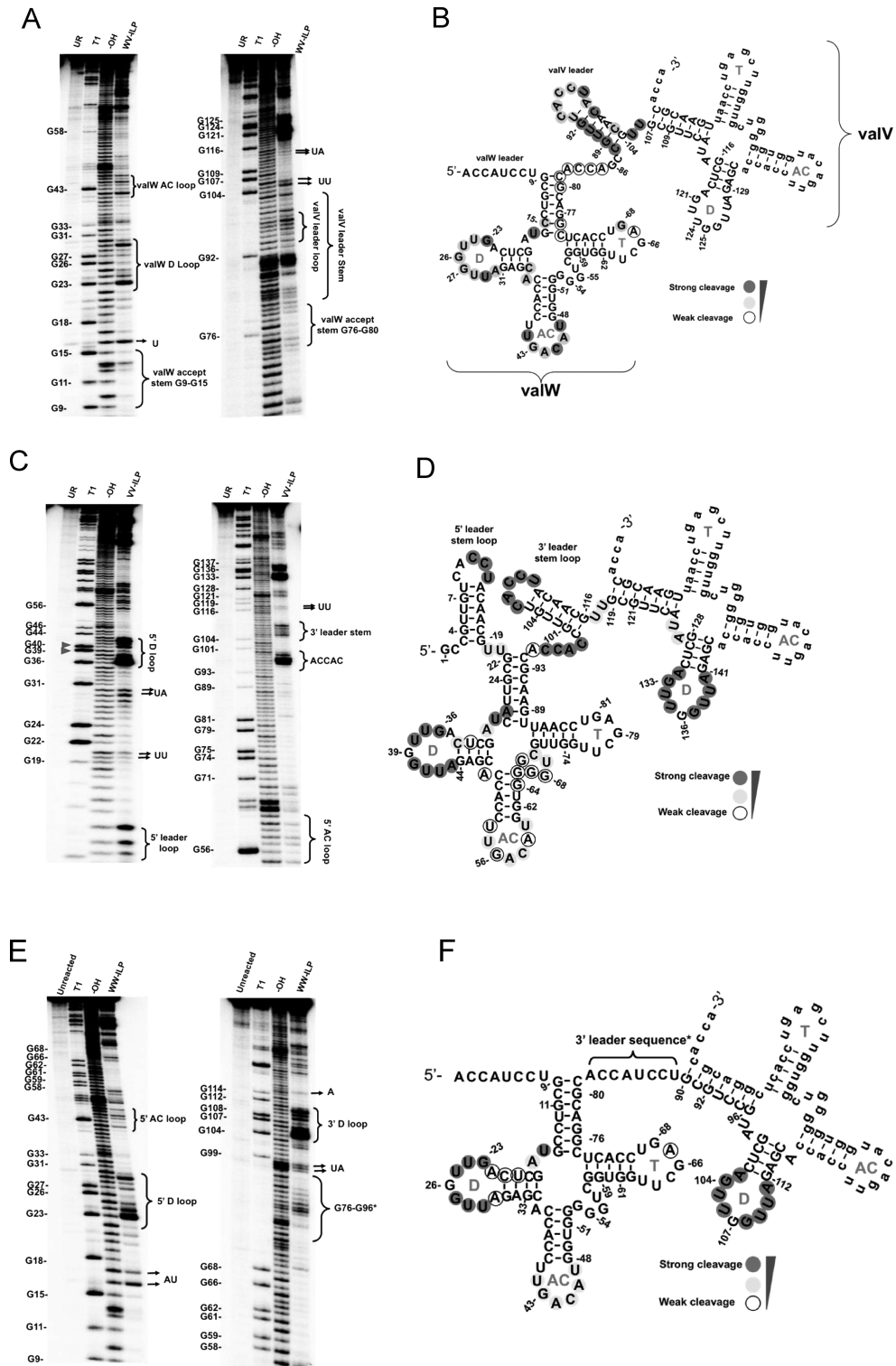


Figure 8. In-line structure probing of 5' end labeled dicentric valWV (A, B), valVV (C, D) and valWW (E, F) substrate RNAs. Panels A, C and E show the levels of spontaneous RNA cleavage at patterns observed with 5' ³²P end-labeled RNAs resolved on 12% and 8% polyacrylamide gels. Lanes are indicated above the gel as follows. NR: unreacted RNA; T1: partial RNase T1 digestion; OH: partial alkaline hydrolysis; WW/ILP: in-line probing reaction. Bands corresponding to certain T1 digestion and alkaline hydrolysis are circled on the predicted secondary structures of valWV, valVV, and valWW in panels B, C and D, respectively.

cursors. In order to quantify differences in RNase P specificity, the values of the observed rate constants were measured under the same single turnover conditions used in kinetic analyses of the native dicistronic substrate. The rate constants summarized in Figure 9 were measured under limiting enzyme concentrations such that the k_{obs} values for RNase P cleavage reflect the activation energy for reaction from an equivalent ground state, i.e. the free substrates in solution. Both the valV and valW ptRNA substrates are processed with essentially identical rate constants in the context of both monocistronic and dicistronic context. We also observed little effect of the presence of the additional four nucleotides at the 3' end of valV that are present in the intermediate **b** resulting from cleavage at the downstream valW cleavage site in the native valVW substrate.

Importantly, the k_{obs} value for RNase P cleavage of the ptRNA^{valV} substrate is consistently 2–4-fold slower than cleavage of ptRNA^{valW} regardless of whether the substrate is processed in the context of a monocistronic or dicistronic substrate. As established by in-line probing experiments, above, a stable stem loop structure clearly forms in the leader of the ptRNA^{valV} substrate. The stem loop includes nucleotides N(-3) to N(-8) which encompass the binding site for the RNase P protein subunit (21,72). As established previously, for a non-initiator ptRNA^{met} substrate the presence of stable secondary structure in the 5' leader sequence can inhibit RNase P processing (34). To test whether the presence of the stem loop inhibits the rate of the monocistronic ptRNA^{valV} the 5' leader sequence was switched with the valW leader 'ACCAUCCU'. Switching the leader sequences with that of ptRNA^{valW} rescues the slower ptRNA^{valV} processing rate, showing that the native leader sequence and associated stem loop structure is likely to inhibit native valV processing. To test this hypothesis, the ability of the ptRNA^{valV} 5' leader to form secondary structure was altered by mutation and the effects on processing rate were measured and compared. The entire stem loop in the genomic encoded valV ptRNA was disrupted to produce a structure-free leader mutation by changing upstream sequence contexts (ptRNA^{valV} mut1, mut2). About 4-fold acceleration in k_{obs} is measured in mut1 when compared to the genomic encoded ptRNA^{valV} 5' leader. However, the k_{obs} measured in the mut2 only have ~1-fold increase in the rate constant, most likely have no significant increase. The entire stem loop then was disrupted and further shortened in length to produce ptRNA^{valV} mut3 and ~4-fold acceleration in k_{obs} is also observed. Since the former three mutations contain the same leader sequence contexts in '-1' to '-8' position, we considered whether sequence specificity in the leader region is also the element responsible for the observed catalysis defect. The ptRNA^{valV} mut4 substrate was generated by disrupting the stem loop by changing the sequences proximal to the cleavage site ('-1' to '-8') to the leader sequence in the ptRNA^{valW} substrate (ACCAUCCU). This substitution results in a similar increase in k_{obs} . Stabilizing the leader structure (ptRNA^{valV} mut5, mut6) by changing sequence contexts of stem or including a stable 'GAAA' tetra loop have no significant effect on the observed cleavage rate.

DISCUSSION

Endoribonucleases that are involved in the initial steps of tRNA and rRNA biosynthesis (e.g. RNase E, RNase P and RNase III) cleave the RNA phosphodiester backbone of their substrates at a specific site, but nonetheless have broad substrate specificity. These RNases are archetypical alternative substrate enzymes because they must recognize many different cognate cleavage sites embedded in different sequence and structure contexts (3,4,11,36–39). In this regard, they reflect a general feature of many RNA binding proteins in that their specificity is broad and physiologically relevant RNA targets may have a range of affinities or may not always be optimized for highest affinity (45,73). The specificity of an enzyme for multiple alternative substrates has two important consequences for understanding the biological function of RNA processing endonucleases. First, their kinetic mechanisms cannot be understood entirely in terms of a simple one enzyme-one substrate reaction schemes. The second is that their specificity cannot be completely defined by approaches that use consensus motif analysis, or that are based entirely on structure-function experiments using only one or a few optimal substrates (45).

Although RNase P is a ribonucleoprotein, there are also other endonucleases involved in stable RNA processing that are protein enzymes. For example, RNase E plays an essential role in mRNA turnover, as well as contributing to rRNA and tRNA maturation and this interacts with numerous RNA target sites (38). Structure-function studies *in vitro* and recent transcriptome-wide identification of RNase E processing sites revealed a sequence signature of a uridine located two nucleotides downstream in a single-stranded segment. However, this motif by itself is insufficient to fully describe RNase E specificity, which may be modulated by other proteins binding to its substrates that sequester binding sites like the site-specific RNA binding protein RsmZ (74), or that help direct cleave at specific sites such as the ubiquitous Hfq (75), or potentially by alteration of RNA location in the cell (38). Like RNase P, the endoribonuclease RNase III has a primary role in cleavage of primary RNA precursors catalysing the first step in rRNA processing, and also plays a global as a dsRNA specific RNA processing enzyme involved in bacterial gene expression and regulation (37,76). Analogous to molecular recognition by RNase P, RNase III does not have a strongly conserved cognate recognition sequence, but instead primarily recognizes elements of dsRNA structure (37,76). Formation of dsRNA containing RNase III target sites is key to regulation of multiple mRNAs encoding proteins involved in environmental stress-related processes (76,77). Competition between alternative binding sites in rRNA and its own gene in the rncO operon is inherent to self-regulation of its expression (78). Variation in regular helical structure among different substrates determines whether one or both strands of a target site will be cleaved (37,79,80). Although the structure and catalytic function of RNase P are well studied, comparatively less is known about its target sites in the transcriptome and potential roles in gene regulation. Genetic depletion studies using microarray analyses to monitor changes in transcript levels suggests control over a range of mRNA processing events, and *in vitro* studies confirm cleavage of

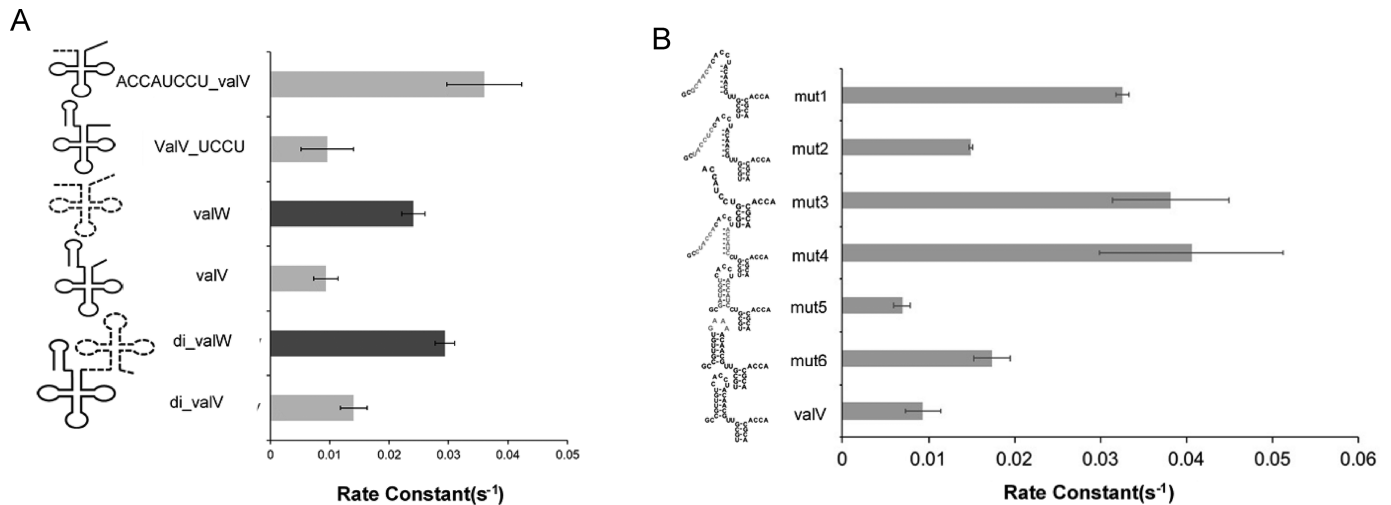


Figure 9. Single turnover reaction analysis of precursor tRNA rate constants. (A) Comparison of rate constants for ptRNA^{valV} and ptRNA^{valW} in mono-cistronic versus dicistronic contexts. The substrate structures are shown on the left. The ptRNA^{valV} substrate is shown as a dashed line and the ptRNA^{valW} is shown as a solid line. (B) Analysis of the effects of leader sequence structure on RNase P processing. The predicted secondary structure of the leader sequences of the individual ptRNA^{valV} mutants are shown on the left.

specific mRNAs and other small RNAs (81–84). However, a complete accounting of RNase P substrates is not yet available.

The *B. subtilis* P RNA encoded by the *rnpB* gene is able to replace and complement a deletion of the homologous *E. coli* RNA subunit despite significant differences in their sequence and secondary structure (85,86). However, growth defects suggest that the function of the hybrid RNase P lacks some key functions of the native *E. coli* enzyme. An important recent advance has been the discovery that RNase P can exist as a ribonucleoprotein or as protein-only enzyme. The single protein form of the enzyme is termed PRORP (PRotein-Only RNase P) and is widespread in the nuclei and organelles of eukaryotes. Indeed, both organellar PRORP and two nuclear PRORP enzymes from *Arabidopsis thaliana* can also confer viability to *E. coli* in which endogenous ribonucleoprotein RNase P has been inactivated (87). However, defects in 4.5S RNA was observed as well as inaccurate processing of ptRNAs with extended acceptor sequences including tRNA^{His} and tRNA^{Sec}, the latter of which was degraded rather than processed in the absence of native ribonucleoprotein RNase P. Despite the potential for compensatory mutations elsewhere in the genome that help confer viability, these enzyme substitution studies led to the conclusion that PRORP enzymes are capable of executing the basic functions of the ribonucleoprotein RNase P enzyme in *Bacteria* and *Eukarya* (87–89). Presumably, these functions include the processing of the dicistronic tRNA^{Val} and tRNA^{Lys} precursor RNAs. It is not known whether the ability of substituting enzymes extends to the property of directional processing, however, it seems unlikely that directional processing is essential. More likely the directional processing is a consequence of the intrinsic substrate specificity of the bacterial enzyme, and any influence on regulation of tRNA levels is likely to be non-essential. Nonetheless, the observation of a range of phenotypes and lower growth rates in the absence of the native *E. coli* enzyme supports the conclusion that, like RNase III and RNase E, the

RNase P ribonucleoprotein plays an important, but not essential role in a range of different RNA regulation pathways.

In addition to shedding light in its biological role, understanding the RNA structures and sequences that direct RNase P cleavage and the mechanistic basis for competition between alternative processing sites for RNase P can provide insight into general principles of RNA processing enzyme specificity. Models of the specificity of RNase P that are useful for understanding its *in vivo* function must include the competition between alternative cognate processing sites. For competition between alternative individual substrates containing single sites several approaches for quantifying relative k_{cat}/K_m values for multiple alternative substrate kinetics *in vitro* have been developed (90–93). The recognition of multiple alternative processing sites in the same RNA transcript will necessarily be subject to the same basic structure-function relationships as single substrates with a few key additional considerations. First, the potential for processivity or facilitated diffusion in which processing of the second site on a transcript is accelerated by limited exchange of the bound enzyme with the free enzyme population. Concepts of facilitated diffusion are well explored for DNA binding proteins and endonucleases (94–96), however, the flexible and complex structure of RNA makes it unlikely that analogous mechanisms apply for site-specific endoribonucleases involved in stable RNA processing. Nonetheless, the electrostatic field generated by large RNAs such as the ribosome can engender unexpectedly fast macromolecular association rates for ribotoxins (97,98). Therefore, it is possible that similar electrostatic association might limit diffusion and accelerate processing at multiple sites on the same RNA precursor. However, the data provided here for the dicistronic valVW demonstrates that RNase P cleavage is non-processive and that directionality processing arises due to the removal of 3' trailer sequences which inhibit processing of the 5' proximal cleavage site.

A key feature of RNase P specificity that is underscored by the results presented here is that the length and structure of the 5' leader and 3' trailer sequences can be important modulators of RNase P specificity. It is now well established that the proximal 5' leader sequence interacts with the essential RNase P protein subunit. These interactions are strongest with single stranded leaders of more than five nucleotides and crosslinking, x-ray crystallography, modelling and *in vitro* structure function studies support leader sequence binding in cleft in the P protein (12,18,21,33,99). Nucleobase specific interactions were identified at N(-4), and high-throughput kinetic analyses demonstrate significant although broad sequence specificity (33,34). The presence of a 5' leader is not essential for tRNA biosynthesis or function *in vivo*, although the length of the leader sequence of suppressor tRNAs can affect growth rate (100). The effects of leader sequence on RNase P recognition are complicated by the potential to form base pairs with the 3' CCA sequence which dramatically slows catalysis and can result in mis-cleavage (101,102). Additionally, the presence of stable secondary structure in the 5' leader proximal to the RNase P cleavage site is inhibitory, although it clearly does not block cleavage, as evidenced by comprehensive analysis of 5' leader specificity of an elongator tRNA^{metT} precursor (34). This effect is clearly supported by the structure-function studies presented here in which a stable stem loop located two nucleotides 5' to the cleavage site results in a *ca.* 10-fold reduction in the observed rate constant for RNase P processing. Thus, the presence or absence of stable structure in the 5' leader sequence within the P protein binding site, as well as the specific sequence of the P protein binding site both contribute to recognition of a particular cleavage site. Together these contributions can be significant resulting in orders of magnitude differences in relative rate constants for RNase P cleavage.

The 3' CCA sequence is encoded in *E. coli* tRNAs genes and therefore included in precursor transcripts (11). Experimental evidence from both *in vivo* and *in vitro* studies demonstrate an important pairing interaction between the RCC sequence located at the tRNA 3' end and the P15 internal bulge in P RNA (103–105). Although it was suggested previously that bacterial RNase P may be inhibited by the presence of long 3' trailer sequences (106), we lack a comprehensive understanding of the contribution of 3' trailer sequences to RNase P specificity. The prevailing view has been that 3' end formation precedes RNase P processing, and until now there has been little motivation to explore such effects for the *E. coli* enzyme. Recently, the presence of a Rho-independent transcription terminator was shown to significantly inhibit the ability of RNase P to process tRNA precursor *in vivo* (10). However, some 3' extensions are benign as demonstrated by the data presented here in which processing of the valV intermediate with an additional four nucleotide AUUA sequence has no effect on relative rate of processing. Additionally, the duplicated dicistronic valVV and valWW substrates are processed efficiently at the 5' proximal RNase P cleavage site despite the presence of a long 3' trailer sequence. However, the fact that these substrates do not fold into uniform structures makes it difficult to understand the basis for these effects. Nonetheless, the data presented here support the conclusion that the pres-

ence of an extended and highly structured 3' trailer sequence reduces the relative rate constant for RNase P processing.

The basic outline of the process of tRNA biosynthesis is understood, and the overall regulation of translation by the stringent response is known. However, the mechanisms by which cells establish the appropriate levels of tRNA by balancing expression and turnover are less well understood. Recent studies make clear that tRNA levels are likely to be dynamically regulated in bacteria including *E. coli* to match the demands of protein synthesis, and that mis-regulation can affect translation efficiency and cell function (57–59,107). The tRNA processing pathways in *E. coli* appear to be stochastic at some level, but different tRNA precursors follow different processing pathways and the consequences of these differences for tRNA gene expression are not known. The ordered processing of dicistronic tRNAs by RNase P offers the potential for coordinated control by changes in RNase P activity. The Pan lab used microarray analysis to show that mature tRNA levels in *B. subtilis* are established by rates of synthesis, processing as well as turnover of precursor and mature tRNAs. Recently it was shown that tRNA precursors originating from the internal spacer regions of the *rrn* operons, in particular, *rrnB* are abundant poly(A) polymerase targets (108). Polyadenylation initiates RNA turnover, so the fact that tRNA precursors are substrates for polyadenylation supports the idea that tRNA levels are regulated at some level by precursor turnover. The directional processing by RNase P provides the potential for coordinated regulation of the dicistronic tRNA operons for valine and lysine tRNAs. Reduced rates of RNase P processing could result in greater turnover of the precursor and therefore lower tRNA abundance. Indeed, proteins involved in stable RNA biosynthesis and degradation are colocalized (although it is not clear if RNase P is involved) and such compartmentalization provides a way to functionally co-ordinate these processes (109).

In the present study, the mechanism for directional processing of dicistronic precursor tRNAs by *E. coli* RNase P was investigated and established to follow a non-processive mechanism. Inhibition of processing by the presence of highly structured 3' trailer sequences appears to be the primary mechanism by which directional processing is established for the dicistronic ptRNA^{val} VW. However, this cannot be the entire story since this mechanism does not explain the directional processing of precursors like valU and lysT that contain four and seven tRNAs, respectively. In these cases, there may be local sequence variations that help to maintain directional processing due to variation or structure in the 5' leader or formation of local inhibitory structure near the cleavage site.

SUPPLEMENTARY DATA

Supplementary Data are available at NAR Online.

FUNDING

National Institutes of Health (NIH) [GM012700 to M.E.H.]. Funding for open access charge: NIH.

Conflict of interest statement. None declared.

REFERENCES

1. Blattner, F.R., Plunkett, G. 3rd, Bloch, C.A., Perna, N.T., Burland, V., Riley, M., Collado-Vides, J., Glasner, J.D., Rode, C.K., Mayhew, G.F. et al. (1997) The complete genome sequence of *Escherichia coli* K-12. *Science*, **277**, 1453–1462.
2. Agrawal, A., Mohanty, B.K. and Kushner, S.R. (2014) Processing of the seven valine tRNAs in *Escherichia coli* involves novel features of RNase P. *Nucleic Acids Res.*, **42**, 11166–11179.
3. Li, Z. and Deutscher, M.P. (1996) Maturation pathways for *E. coli* tRNA precursors: a random multienzyme process in vivo. *Cell*, **86**, 503–512.
4. Li, Z. and Deutscher, M.P. (2002) RNase E plays an essential role in the maturation of *Escherichia coli* tRNA precursors. *RNA*, **8**, 97–109.
5. Mohanty, B.K. and Kushner, S.R. (2007) Ribonuclease P processes polycistronic tRNA transcripts in *Escherichia coli* independent of ribonuclease E. *Nucleic Acids Res.*, **35**, 7614–7625.
6. Mohanty, B.K. and Kushner, S.R. (2010) Processing of the *Escherichia coli* leuX tRNA transcript, encoding tRNA(Leu5), requires either the 3'→5' exonuclease polynucleotide phosphorylase or RNase P to remove the Rho-independent transcription terminator. *Nucleic Acids Res.*, **38**, 597–607.
7. Ow, M.C. and Kushner, S.R. (2002) Initiation of tRNA maturation by RNase E is essential for cell viability in *E. coli*. *Genes Dev.*, **16**, 1102–1115.
8. Ziehler, W.A., Day, J.J., Fierke, C.A. and Engelke, D.R. (2000) Effects of 5' leader and 3' trailer structures on pre-tRNA processing by nuclear RNase P. *Biochemistry*, **39**, 9909–9916.
9. Gossringer, M., Helmecke, D. and Hartmann, R.K. (2012) Characterization of RNase P RNA activity. *Methods Mol. Biol.*, **848**, 61–72.
10. Mohanty, B.K. and Kushner, S.R. (2008) Rho-independent transcription terminators inhibit RNase P processing of the secG leuU and metT tRNA polycistronic transcripts in *Escherichia coli*. *Nucleic Acids Res.*, **36**, 364–375.
11. Shepherd, J. and Ibbas, M. (2015) Bacterial transfer RNAs. *FEMS Microbiol. Rev.*, **39**, 280–300.
12. Klemm, B.P., Wu, N., Chen, Y., Liu, X., Kaitany, K.J., Howard, M.J. and Fierke, C.A. (2016) The diversity of Ribonuclease P: Protein and RNA catalysts with analogous biological functions. *Biomolecules*, **6**, E27.
13. Howard, M.J., Liu, X., Lim, W.H., Klemm, B.P., Fierke, C.A., Koutmos, M. and Engelke, D.R. (2013) RNase P enzymes: divergent scaffolds for a conserved biological reaction. *RNA Biol.*, **10**, 909–914.
14. Evans, D., Marquez, S.M. and Pace, N.R. (2006) RNase P: interface of the RNA and protein worlds. *Trends Biochem. Sci.*, **31**, 333–341.
15. Jarrous, N. and Gopalan, V. (2010) Archaeal/eukaryal RNase P: subunits, functions and RNA diversification. *Nucleic Acids Res.*, **38**, 7885–7894.
16. Tsai, H.Y., Masquida, B., Biswas, R., Westhof, E. and Gopalan, V. (2003) Molecular modeling of the three-dimensional structure of the bacterial RNase P holoenzyme. *J. Mol. Biol.*, **325**, 661–675.
17. Frank, D.N. and Pace, N.R. (1998) Ribonuclease P: unity and diversity in a tRNA processing ribozyme. *Annu. Rev. Biochem.*, **67**, 153–180.
18. Reiter, N.J., Osterman, A., Torres-Larios, A., Swinger, K.K., Pan, T. and Mondragon, A. (2010) Structure of a bacterial ribonuclease P holoenzyme in complex with tRNA. *Nature*, **468**, 784–789.
19. Harris, M.E., Kazantsev, A.V., Chen, J.L. and Pace, N.R. (1997) Analysis of the tertiary structure of the ribonuclease P ribozyme-substrate complex by site-specific photoaffinity crosslinking. *RNA*, **3**, 561–576.
20. Harris, M.E., Nolan, J.M., Malhotra, A., Brown, J.W., Harvey, S.C. and Pace, N.R. (1994) Use of photoaffinity crosslinking and molecular modeling to analyze the global architecture of ribonuclease P RNA. *EMBO J.*, **13**, 3953–3963.
21. Kurz, J.C., Niranjanakumari, S. and Fierke, C.A. (1998) Protein component of *Bacillus subtilis* RNase P specifically enhances the affinity for precursor-tRNA. *Biochemistry*, **37**, 2393–2400.
22. Kurz, J.C. and Fierke, C.A. (2002) The affinity of magnesium binding sites in the *Bacillus subtilis* RNase P x pre-tRNA complex is enhanced by the protein subunit. *Biochemistry*, **41**, 9545–9558.
23. Sun, L. and Harris, M.E. (2007) Evidence that binding of C5 protein to P RNA enhances ribozyme catalysis by influencing active site metal ion affinity. *RNA*, **13**, 1505–1515.
24. Koutmou, K.S., Day-Storms, J.J. and Fierke, C.A. (2011) The RNR motif of *B. subtilis* RNase P protein interacts with both PRNA and pre-tRNA to stabilize an active conformer. *RNA*, **17**, 1225–1235.
25. Buck, A.H., Kazantsev, A.V., Dalby, A.B. and Pace, N.R. (2005) Structural perspective on the activation of RNase P RNA by protein. *Nat. Struct. Mol. Biol.*, **12**, 958–964.
26. Buck, A.H., Dalby, A.B., Poole, A.W., Kazantsev, A.V. and Pace, N.R. (2005) Protein activation of a ribozyme: the role of bacterial RNase P protein. *EMBO J.*, **24**, 3360–3368.
27. Lechner, M., Rossmanith, W., Hartmann, R.K., Tholken, C., Gutmann, B., Giege, P. and Gobert, A. (2015) Distribution of ribonucleoprotein and protein-only RNase P in Eukarya. *Mol. Biol. Evol.*, **32**, 3186–3193.
28. Pan, T., Loria, A. and Zhong, K. (1995) Probing of tertiary interactions in RNA: 2'-hydroxyl-base contacts between the RNase P RNA and pre-tRNA. *Proc. Natl. Acad. Sci. U.S.A.*, **92**, 12510–12514.
29. Gaur, R.K. and Krupp, G. (1993) Modification interference approach to detect ribose moieties important for the optimal activity of a ribozyme. *Nucleic Acids Res.*, **21**, 21–26.
30. Suwa, S., Nagai, Y., Fujimoto, A., Kikuchi, Y. and Tanaka, T. (2009) Analysis on substrate specificity of *Escherichia coli* ribonuclease P using shape variants of pre-tRNA: proposal of subsites model for substrate shape recognition. *J. Biochem.*, **145**, 151–160.
31. Loria, A. and Pan, T. (2000) The 3' substrate determinants for the catalytic efficiency of the *Bacillus subtilis* RNase P holoenzyme suggest autolytic processing of the RNase P RNA in vivo. *RNA*, **6**, 1413–1422.
32. Wu, S., Chen, Y., Lindell, M., Mao, G. and Kirsebom, L.A. (2011) Functional coupling between a distal interaction and the cleavage site in bacterial RNase-P-RNA-mediated cleavage. *J. Mol. Biol.*, **411**, 384–396.
33. Koutmou, K.S., Zahler, N.H., Kurz, J.C., Campbell, F.E., Harris, M.E. and Fierke, C.A. (2010) Protein-precursor tRNA contact leads to sequence-specific recognition of 5' leaders by bacterial ribonuclease P. *J. Mol. Biol.*, **396**, 195–208.
34. Lin, H.C., Zhao, J., Niland, C.N., Tran, B., Jankowsky, E. and Harris, M.E. (2016) Analysis of the RNA Binding Specificity Landscape of C5 Protein Reveals Structure and Sequence Preferences that Direct RNase P Specificity. *Cell Chem. Biol.*, **23**, 1271–1281.
35. Altuvia, Y., Bar, A., Reiss, N., Karavani, E., Argaman, L. and Margalit, H. (2018) In vivo cleavage rules and target repertoire of RNase III in *Escherichia coli*. *Nucleic Acids Res.*, **46**, 10380–10394.
36. Deutscher, M.P. (2009) Maturation and degradation of ribosomal RNA in bacteria. *Prog. Mol. Biol. Transl. Sci.*, **85**, 369–391.
37. Nicholson, A.W. (2014) Ribonuclease III mechanisms of double-stranded RNA cleavage. *Wiley Interdiscip. Rev. RNA*, **5**, 31–48.
38. Mackie, G.A. (2013) RNase E: at the interface of bacterial RNA processing and decay. *Nat. Rev. Microbiol.*, **11**, 45–57.
39. Deutscher, M.P. (2009) In: *Progress in Molecular Biology and Translational Science*. Academic Press, Vol. **85**, pp. 369–391.
40. Taliaferro, J.M., Lambert, N.J., Sudmant, P.H., Dominguez, D., Merkin, J.J., Alexis, M.S., Bazile, C. and Burge, C.B. (2016) RNA sequence context effects measured in vitro predict in vivo protein binding and regulation. *Mol. Cell*, **64**, 294–306.
41. Fu, X.D. and Ares, M. Jr (2014) Context-dependent control of alternative splicing by RNA-binding proteins. *Nat. Rev. Genet.*, **15**, 689–701.
42. Pickering, B.M. and Willis, A.E. (2005) The implications of structured 5' untranslated regions on translation and disease. *Semin. Cell Dev. Biol.*, **16**, 39–47.
43. Lin, C.L., Taggart, A.J. and Fairbrother, W.G. (2016) RNA structure in splicing: an evolutionary perspective. *RNA Biol.*, **13**, 766–771.
44. Barash, Y., Calarco, J.A., Gao, W., Pan, Q., Wang, X., Shai, O., Blencowe, B.J. and Frey, B.J. (2010) Deciphering the splicing code. *Nature*, **465**, 53–59.
45. Jankowsky, E. and Harris, M.E. (2015) Specificity and nonspecificity in RNA-protein interactions. *Nat. Rev. Mol. Cell Biol.*, **16**, 533–544.

46. Manning, K.S. and Cooper, T.A. (2017) The roles of RNA processing in translating genotype to phenotype. *Nat. Rev. Mol. Cell Biol.*, **18**, 102–114.
47. Zarnack, K., Konig, J., Tajnik, M., Martincorena, I., Eustermann, S., Stevant, I., Reyes, A., Anders, S., Luscombe, N.M. and Ule, J. (2013) Direct competition between hnRNP C and U2AF65 protects the transcriptome from the exonization of Alu elements. *Cell*, **152**, 453–466.
48. Sellier, C., Cerro-Herreros, E., Blatter, M., Freyermuth, F., Gaucherot, A., Ruffenach, F., Sarkar, P., Puymirat, J., Udd, B. and Day, J.W. (2018) rbFOX1/MBNL1 competition for CCUG RNA repeats binding contributes to myotonic dystrophy type 1/type 2 differences. *Nat. Commun.*, **9**, 2009.
49. Nazim, M., Masuda, A., Rahman, M.A., Nasrin, F., Takeda, J.-I., Ohe, K., Ohkawara, B., Ito, M. and Ohno, K. (2017) Competitive regulation of alternative splicing and alternative polyadenylation by hnRNP H and CstF64 determines acetylcholinesterase isoforms. *Nucleic Acids Res.*, **45**, 1455–1468.
50. Dassi, E. (2017) Handshakes and fights: the regulatory interplay of RNA-binding proteins. *Front. Mol. Biosci.*, **4**, 67.
51. Yu, T.X., Rao, J.N., Zou, T., Liu, L., Xiao, L., Ouyang, M., Cao, S., Gorospe, M. and Wang, J.Y. (2013) Competitive binding of CUGBP1 and HuR to occludin mRNA controls its translation and modulates epithelial barrier function. *Mol. Biol. Cell*, **24**, 85–99.
52. Elkon, R., Ugalde, A.P. and Agami, R. (2013) Alternative cleavage and polyadenylation: extent, regulation and function. *Nat. Rev. Genet.*, **14**, 496–506.
53. Warf, M.B., Diegel, J.V., von Hippel, P.H. and Berglund, J.A. (2009) The protein factors MBNL1 and U2AF65 bind alternative RNA structures to regulate splicing. *Proc. Natl. Acad. Sci. U.S.A.*, **106**, 9203–9208.
54. Foley, S.W., Kramer, M.C. and Gregory, B.D. (2017) RNA structure, binding, and coordination in Arabidopsis. *Wiley Interdiscip. Rev RNA*, **8**, 1426–1446.
55. Liu, N., Zhou, K.I., Parisien, M., Dai, Q., Diatchenko, L. and Pan, T. (2017) N6-methyladenosine alters RNA structure to regulate binding of a low-complexity protein. *Nucleic Acids Res.*, **45**, 6051–6063.
56. Huang, H., Zhang, J., Harvey, S.E., Hu, X. and Cheng, C. (2017) RNA G-quadruplex secondary structure promotes alternative splicing via the RNA-binding protein hnRNP. *Genes Dev.*, **31**, 2296–2309.
57. Dong, H., Nilsson, L. and Kurland, C.G. (1996) Co-variation of tRNA abundance and codon usage in Escherichia coli at different growth rates. *J. Mol. Biol.*, **260**, 649–663.
58. Sørensen, M.A., Fehler, A.O. and Lo Svenningsen, S. (2018) Transfer RNA instability as a stress response in Escherichia coli: Rapid dynamics of the tRNA pool as a function of demand. *RNA Biol.*, **15**, 586–593.
59. Svenningsen, S.L., Kongstad, M., Stenum, T.S., Munoz-Gomez, A.J. and Sorensen, M.A. (2017) Transfer RNA is highly unstable during early amino acid starvation in Escherichia coli. *Nucleic Acids Res.*, **45**, 793–804.
60. Dittmar, K.A., Goodenbour, J.M. and Pan, T. (2006) Tissue-specific differences in human transfer RNA expression. *PLoS Genet.*, **2**, e221.
61. Dittmar, K.A., Mobley, E.M., Radek, A.J. and Pan, T. (2004) Exploring the regulation of tRNA distribution on the genomic scale. *J. Mol. Biol.*, **337**, 31–47.
62. Guo, X., Campbell, F.E., Sun, L., Christian, E.L., Anderson, V.E. and Harris, M.E. (2006) RNA-dependent folding and stabilization of C5 protein during assembly of the E. coli RNase P holoenzyme. *J. Mol. Biol.*, **360**, 190–203.
63. Christian, E.L., McPheeters, D.S. and Harris, M.E. (1998) Identification of individual nucleotides in the bacterial ribonuclease P ribozyme adjacent to the pre-tRNA cleavage site by short-range photo-cross-linking. *Biochemistry*, **37**, 17618–17628.
64. Christian, E.L., Zahler, N.H., Kaye, N.M. and Harris, M.E. (2002) Analysis of substrate recognition by the ribonucleoprotein endonuclease RNase P. *Methods*, **28**, 307–322.
65. Huang, C. and Yu, Y.T. (2013) Synthesis and labeling of RNA in vitro. *Curr. Protoc. Mol. Biol.*, doi:10.1002/0471142727.mb0415s102.
66. Fersht, A. (1998) *Structure and Mechanism in Protein Science*. W.H. Freeman & Co.
67. Regulski, E.E. and Breaker, R.R. (2008) In-line probing analysis of riboswitches. *Methods Mol. Biol.*, **419**, 53–67.
68. Rose, I.A., O'Connell, E.L. and Litwin, S. (1974) Determination of the rate of hexokinase-glucose dissociation by the isotope-trapping method. *J. Biol. Chem.*, **249**, 5163–5168.
69. Yandek, L.E., Lin, H.C. and Harris, M.E. (2013) Alternative substrate kinetics of Escherichia coli ribonuclease P: determination of relative rate constants by internal competition. *J. Biol. Chem.*, **288**, 8342–8354.
70. Milligan, J.F., Groebe, D.R., Witherell, G.W. and Uhlenbeck, O.C. (1987) Oligoribonucleotide synthesis using T7 RNA polymerase and synthetic DNA templates. *Nucleic Acids Res.*, **15**, 8783–8798.
71. Milligan, J.F. and Uhlenbeck, O.C. (1989) Synthesis of small RNAs using T7 RNA polymerase. *Methods Enzymol.*, **180**, 51–62.
72. Sun, L., Campbell, F.E., Yandek, L.E. and Harris, M.E. (2010) Binding of C5 protein to P RNA enhances the rate constant for catalysis of P RNA processing of pre-tRNAs lacking a consensus (+1)/C(+72) pair. *J. Mol. Biol.*, **395**, 1019–1037.
73. Helder, S., Blythe, A.J., Bond, C.S. and Mackay, J.P. (2016) Determinants of affinity and specificity in RNA-binding proteins. *Curr. Opin. Struct. Biol.*, **38**, 83–91.
74. Duss, G., Michel, E., Yulikov, M., Schubert, M., Jeschke, G. and Allain, F.H.T. (2014) Structural basis of the non-coding RNA RsmZ acting as a protein sponge. *Nature*, **509**, 588.
75. Chao, Y., Li, L., Girodat, D., Forstner, K.U., Said, N., Corcoran, C., Smiga, M., Papenfort, K., Reinhardt, R., Wieden, H.J. et al. (2017) In Vivo Cleavage Map Illuminates the Central Role of RNase E in Coding and Non-coding RNA Pathways. *Mol. Cell*, **65**, 39–51.
76. Lim, B., Sim, M., Lee, H., Hyun, S., Lee, Y., Hahn, Y., Shin, E. and Lee, K. (2015) Regulation of Escherichia coli RNase III activity. *J. Microbiol.*, **53**, 487–494.
77. Lalaouna, D., Simoneau-Roy, M., Lafontaine, D. and Masse, E. (2013) Regulatory RNAs and target mRNA decay in prokaryotes. *Biochim. Biophys. Acta*, **1829**, 742–747.
78. Matsunaga, J., Simons, E.L. and Simons, R.W. (1996) RNase III autoregulation: structure and function of rncO, the posttranscriptional “operator”. *RNA*, **2**, 1228–1240.
79. Pertz, A.V. and Nicholson, A.W. (2006) Characterization of RNA sequence determinants and antideterminants of processing reactivity for a minimal substrate of Escherichia coli ribonuclease III. *Nucleic Acids Res.*, **34**, 3708–3721.
80. Chelladurai, B., Li, H., Zhang, K. and Nicholson, A.W. (1993) Mutational analysis of a ribonuclease III processing signal. *Biochemistry*, **32**, 7549–7558.
81. Altman, S., Wesolowski, D., Guerrier-Takada, C. and Li, Y. (2005) RNase P cleaves transient structures in some riboswitches. *PNAS*, **102**, 11284–11289.
82. Hartmann, R.K., Heinrich, J., Schlegel, J. and Schuster, H. (1995) Precursor of C4 antisense RNA of bacteriophages P1 and P7 is a substrate for RNase P of Escherichia coli. *Proc. Natl. Acad. Sci. U.S.A.*, **92**, 5822–5826.
83. Li, Y. and Altman, S. (1996) Cleavage by RNase P of gene N mRNA reduces bacteriophage lambda burst size. *Nucleic Acids Res.*, **24**, 835–842.
84. Li, Y. and Altman, S. (2003) A specific endoribonuclease, RNase P, affects gene expression of polycistronic operon mRNAs. *Proc. Natl. Acad. Sci. U.S.A.*, **100**, 13213–13218.
85. Waugh, D.S. and Pace, N.R. (1990) Complementation of an RNase P RNA (rnpB) gene deletion in Escherichia coli by homologous genes from distantly related eubacteria. *J. Bacteriol.*, **172**, 6316–6322.
86. Wegscheid, B., Condon, C. and Hartmann, R.K. (2006) Type A and B RNase P RNAs are interchangeable in vivo despite substantial biophysical differences. *EMBO Rep.*, **7**, 411–417.
87. Gossringer, M., Lechner, M., Brillante, N., Weber, C., Rossmannith, W. and Hartmann, R.K. (2017) Protein-only RNase P function in Escherichia coli: viability, processing defects and differences between PRORP isoenzymes. *Nucleic Acids Res.*, **45**, 7441–7454.
88. Taschner, A., Weber, C., Buzet, A., Hartmann, R.K., Hartig, A. and Rossmannith, W. (2012) Nuclear RNase P of Trypanosoma brucei: a single protein in place of the multicomponent RNA-protein complex. *Cell Rep.*, **2**, 19–25.
89. Weber, C., Hartig, A., Hartmann, R.K. and Rossmannith, W. (2014) Playing RNase P Evolution: Swapping the RNA catalyst for a

- protein reveals functional uniformity of highly divergent enzyme forms. *PLoS Genet.*, **10**, e1004506.
90. Anderson, V.E. (2015) Multiple alternative substrate kinetics. *Biochim. Biophys. Acta*, **1854**, 1729–1736.
 91. Kuo, Y.M., Henry, R.A. and Andrews, A.J. (2016) Measuring specificity in multi-substrate/product systems as a tool to investigate selectivity in vivo. *Biochim. Biophys. Acta*, **1864**, 70–76.
 92. Schellenberger, V., Siegel, R.A. and Rutter, W.J. (1993) Analysis of enzyme specificity by multiple substrate kinetics. *Biochemistry*, **32**, 4344–4348.
 93. Deng, Z., Mao, J., Wang, Y., Zou, H. and Ye, M. (2017) Enzyme kinetics for complex system enables accurate determination of specificity constants of numerous substrates in a mixture by proteomics platform. *Mol. Cell. Proteomics.*, **16**, 135–145.
 94. Kolomeisky, A.B. (2011) Physics of protein-DNA interactions: mechanisms of facilitated target search. *Phys. Chem. Chem. Phys.*, **13**, 2088–2095.
 95. Siggers, T. and Gordan, R. (2014) Protein-DNA binding: complexities and multi-protein codes. *Nucleic Acids Res.*, **42**, 2099–2111.
 96. von Hippel, P.H. and Berg, O.G. (1989) Facilitated target location in biological systems. *J. Biol. Chem.*, **264**, 675–678.
 97. Korennykh, A.V., Piccirilli, J.A. and Correll, C.C. (2006) The electrostatic character of the ribosomal surface enables extraordinarily rapid target location by ribotoxins. *Nat. Struct. Mol. Biol.*, **13**, 436–443.
 98. Plantinga, M.J., Korennykh, A.V., Piccirilli, J.A. and Correll, C.C. (2008) Electrostatic interactions guide the active site face of a structure-specific ribonuclease to its RNA substrate. *Biochemistry*, **47**, 8912–8918.
 99. Niranjankumari, S., Day-Storms, J.J., Ahmed, M., Hsieh, J., Zahler, N.H., Venters, R.A. and Fierke, C.A. (2007) Probing the architecture of the *B. subtilis* RNase P holoenzyme active site by cross-linking and affinity cleavage. *RNA*, **13**, 521–535.
 100. Fredrik Pettersson, B.M., Ardell, D.H. and Kirsebom, L.A. (2005) The length of the 5' leader of *Escherichia coli* tRNA precursors influences bacterial growth. *J. Mol. Biol.*, **351**, 9–15.
 101. Brannvall, M., Kikovska, E. and Kirsebom, L.A. (2004) Cross talk between the +73/294 interaction and the cleavage site in RNase P RNA mediated cleavage. *Nucleic Acids Res.*, **32**, 5418–5429.
 102. Kikovska, E., Brannvall, M. and Kirsebom, L.A. (2006) The exocyclic amine at the RNase P cleavage site contributes to substrate binding and catalysis. *J. Mol. Biol.*, **359**, 572–584.
 103. Brannvall, M., Pettersson, B.M. and Kirsebom, L.A. (2003) Importance of the +73/294 interaction in *Escherichia coli* RNase P RNA substrate complexes for cleavage and metal ion coordination. *J. Mol. Biol.*, **325**, 697–709.
 104. Busch, S., Kirsebom, L.A., Notbohm, H. and Hartmann, R.K. (2000) Differential role of the intermolecular base-pairs G292-C(75) and G293-C(74) in the reaction catalyzed by *Escherichia coli* RNase P RNA. *J. Mol. Biol.*, **299**, 941–951.
 105. Kirsebom, L.A. and Svard, S.G. (1994) Base pairing between *Escherichia coli* RNase P RNA and its substrate. *EMBO J.*, **13**, 4870–4876.
 106. Altman, S., Baer, M., Gold, H., Guerrier-Takada, C., Kirsebom, L., Lawrence, N., Lumelsky, N. and Vioque, A. (1987) *Cleavage of RNA by RNase P from Escherichia coli*.
 107. Kramer, E.B. and Farabaugh, P.J. (2007) The frequency of translational misreading errors in *E. coli* is largely determined by tRNA competition. *RNA*, **13**, 87–96.
 108. Alexandre, M., Céline, G., Eliane, H. and Philippe, R. (2012) Search for poly(A) polymerase targets in *E. coli* reveals its implication in surveillance of Glu tRNA processing and degradation of stable RNAs. *Mol. Microbiol.*, **83**, 436–451.
 109. Taghbalout, A., Yang, Q. and Arluison, V. (2014) The *Escherichia coli* RNA processing and degradation machinery is compartmentalized within an organized cellular network. *Biochem. J.*, **458**, 11–22.